Chapter 2

AN EXCEPTIONALLY DAMAGE-TOLERANT GLASS

ABSTRACT

Owing to a lack of microstructure, glassy materials are inherently strong but brittle, and often demonstrate extreme sensitivity to flaws. Accordingly, their macroscopic failure is often not initiated by plastic yielding, and almost always terminated by brittle fracture. Unlike conventional brittle glasses, metallic glasses are generally capable of limited plastic yielding by shear-band sliding in the vicinity of a flaw, and thus exhibit toughness–strength relationships that lie between brittle ceramics and marginally tough metals. Here, a bulk glassy Pd-alloy is introduced demonstrating an unusual capacity for shielding an opening crack accommodated by an extensive shear-band sliding process, which promotes a fracture toughness comparable to the toughest materials known. This result demonstrates that the combination of toughness and strength (i.e., damage tolerance) accessible to amorphous materials extends beyond the benchmark ranges established by the toughest and strongest materials known, thereby pushing the envelope of damage tolerance accessible to a structural metal.

INTRODUCTION

Crystalline materials exhibit ordered structures with morphological features (e.g., grains) that usually extend to the microscopic level. The defects associated with those microstructural features (e.g., dislocations) become mobile under stress, enabling extensive plastic shielding ahead of an opening crack, which promotes high fracture toughness. The elastic energy threshold for those defects to become active, however, is often low, resulting in rather low yield strengths. For example, ductile metals (e.g., low-carbon steels) have very high fracture toughness (>200 $MPa \cdot m^{1/2}$), but fairly low plastic yield strength (<500 MPa). By contrast, a material with an amorphous atomic structure that lacks microstructural defects has the potential to yield plastically at much higher strengths. Because of the absence of those defects, however, the attainable plasticity ahead of an opening crack tip is limited, and consequently, an opening flaw is often accommodated by unstable crack propagation resulting in low fracture toughness. For example, oxide glasses such as silicates have very high estimated yield strengths (up to 3 GPa) but lack any substantial toughness (<1 $MPa \cdot m^{1/2}$), and consequently, their failure is accommodated by brittle fracture occurring well below the theoretical yield strength (<100 MPa). In this regard, the properties of toughness and strength are invariably mutually exclusive in essentially all classes of materials [1]. This inherent trade-off between strength and toughness is the fundamental challenge in the quest for highly damage-tolerant materials [2]. To date, some success has been achieved through development of composite microstructures, which typically combine a strong glassy matrix with ductile crystalline reinforcements at structural length scales that suppress fracture while maintaining high

strength [3]. Achieving combinations of strength and toughness that fall outside the benchmarks of traditional structural metals, however, remains an outstanding challenge. In this work, a monolithic metallic glass alloy is introduced demonstrating a level of damage tolerance previously inaccessible to the toughest and strongest engineering materials known.

Unlike brittle oxide glasses, metallic glasses are more likely to yield plastically under an opening stress. Consequently, most metallic glasses demonstrate substantial fracture toughness, and strengths consistent with the limit of elasticity of the amorphous structure (~2% of Young's modulus). Toughness–strength data reported to date for metallic glasses bridge the gap between brittle ceramics and marginally tough metals [4-6]. Specifically, reported fracture toughness values range from just over 1 $MPa \cdot m^{1/2}$ (for brittle rare-earth and ferrous metal glasses) [7,8] to about 100 $MPa \cdot m^{1/2}$ (for tougher noble and early-transition metal glasses) [9-11]. Reported strengths vary from about 0.5 GPa (for weak rare-earth metal glasses) [7] to as high as 5 GPa (for strong ferrous metal glasses) [12]. As demonstrated here, the toughness potentially accessible to an amorphous metal in fact extends much further, approaching values characteristic of the toughest materials known, while strengths consistent with the elasticity of the amorphous structure are retained.

Mechanistically, when an opening stress on the order of the material yield strength is applied, plastic shear sliding ensues confined within nanoscopic bands (shear bands) oriented along planes of maximum resolved shear stress. Such shear bands propagate by slip under negative pressure up to some critical shear strain, beyond which they open into

emerging cracks. Under uniform negative pressure, as in quasi-static uniaxial tension, shear band opening in bulk samples becomes unstable and a crack propagates rapidly across the glassy structure resulting in essentially zero macroscopic plastic strain. In a quasi-stable loading geometry, however, as in bending, shear sliding initiated at the tensile surface can be arrested if propagated to the neutral axis without opening, such that stable plastic deformation can be achieved [13].

On the atomic scale, local shear sliding in the shear band is accommodated by cooperative inelastic rearrangements of local clusters of ~100 atoms [14]. Shearing can be sustained under negative pressure until low-density configurations develop and critical cavities eventually emerge. Upon the intervention of cavitation, plastic shearing is terminated and mechanical energy is dissipated via crack extension [15]. One can therefore expect that the extent to which a glass can undergo shear sliding under negative pressure prior to forming critical cavities should be proportional to its capacity to plastically shield an opening crack, and by extension, to its overall fracture toughness. It is therefore conceivable that very large fracture toughness values are theoretically possible for glasses with a capacity to undergo multiple configurational shear rearrangements prior to forming critical cavities, or equivalently, with activation barriers for shear flow much smaller than the activation barriers for cavitation. The glassy metal introduced here appears to exhibit such capacity, as it demonstrates an unusual propensity for shear flow without cavitation, which promotes very high fracture toughness.

GLASS DEVELOPMENT AND PROCESSING

Bulk-glass formation in Pd-rich metal/metalloid composition space was explored in the current work. The glass forming ability of Pd/metalloid systems was first recognized by Duwez *et al*. in 1965 [16]. Early Pd-rich metal/metalloid systems demonstrated only marginal glass-forming ability, but exhibited a very high Poisson's ratio (approaching 0.42) [17] together with a high glass-transition temperature (in excess of 600 K) [18]; high values for these two properties, as we argue later in the article, designate a high glass toughness. Indeed, a fairly robust fracture resistance was noted for those early marginal glass formers [19,20]. In the present study, Pd-rich metal/metalloid compositions were sought capable of forming bulk glasses while exhibiting Poisson ratios and glass-transition temperatures comparable to those of the early glass formers.

Pd-rich metal/metalloid alloys were prepared by inductively melting the pure elements in quartz tubes under an inert atmosphere. Alloy ingots were fluxed in quartz tubes with anhydrous B_2O_3 at ~1200 K for ~1000 s [21]. To form glassy samples, the fluxed ingots were melted in quartz tubes with 0.5 mm wall thickness and then rapidly quenched in a water bath. The quartz-tube water quenching method was found to be more efficient in terms of glass formation than copper-mold casting. The combination of Pd with P, Si, and Ge at composition $Pd_{82.5}P_6Si_{9.5}Ge_2$ (at%) was found capable of forming glassy rods 1 mm in diameter. Microalloying this composition with Ag was found to dramatically enhance glass formation. Specifically, the alloy $Pd_{79}Ag_{3.5}P_6Si_{9.5}Ge_2$ was found capable of forming glassy rods 6 mm in diameter, a dramatic increase in glass-forming ability.

GLASS CHARACTERIZATION

X-ray diffraction, high-resolution transmission electron microscopy (TEM), and differential scanning calorimetry (DSC) analyses verifying the amorphous structure of the $Pd_{79}Ag_{3.5}P_6Si_{9.5}Ge_2$ glass are presented in figure 2.1. Figure 2.1(a) shows the amorphous X-ray diffraction pattern taken by a Panalytical X'Pert Pro X-ray diffractometer with Cu K_α radiation. The high-resolution TEM image shown in figure 2.1(b) displays the lack of long-range order expected in a fully amorphous sample. The inset of figure 2.1(b) is the selected area diffraction pattern, confirming the amorphous nature with a fully amorphous diffuse ring diffraction pattern. Both images were taken with a field-emission FEI Tecnai F30UT TEM. The DSC scan shown in figure 2.1(c) was performed using a Netzsch Pegasus 404C DSC at a scanning rate of 0.333 °C s^{-1}. The arrows in figure 2.1(c) indicate the glass-transition temperature T_g = 613 K, the crystallization temperature T_x = 644 K, the solidus temperature T_s = 967 K, and the liquidus temperature T_l = 1065 K. The difference between T_g and T_x, termed ΔT, is 31 K and the critical casting diameter is 6 mm. The density of the glass ρ = 10.7 g/cm^3 was measured using the Archimedes buoyancy technique. The shear and longitudinal wave speeds were measured with a 25 MHz transducer via the pulse-echo overlap technique. The wave speeds and density were combined to calculate a shear modulus of 31 GPa and a bulk modulus of 172 GPa, resulting in a satisfactorily high Poisson's ratio of ~0.42.

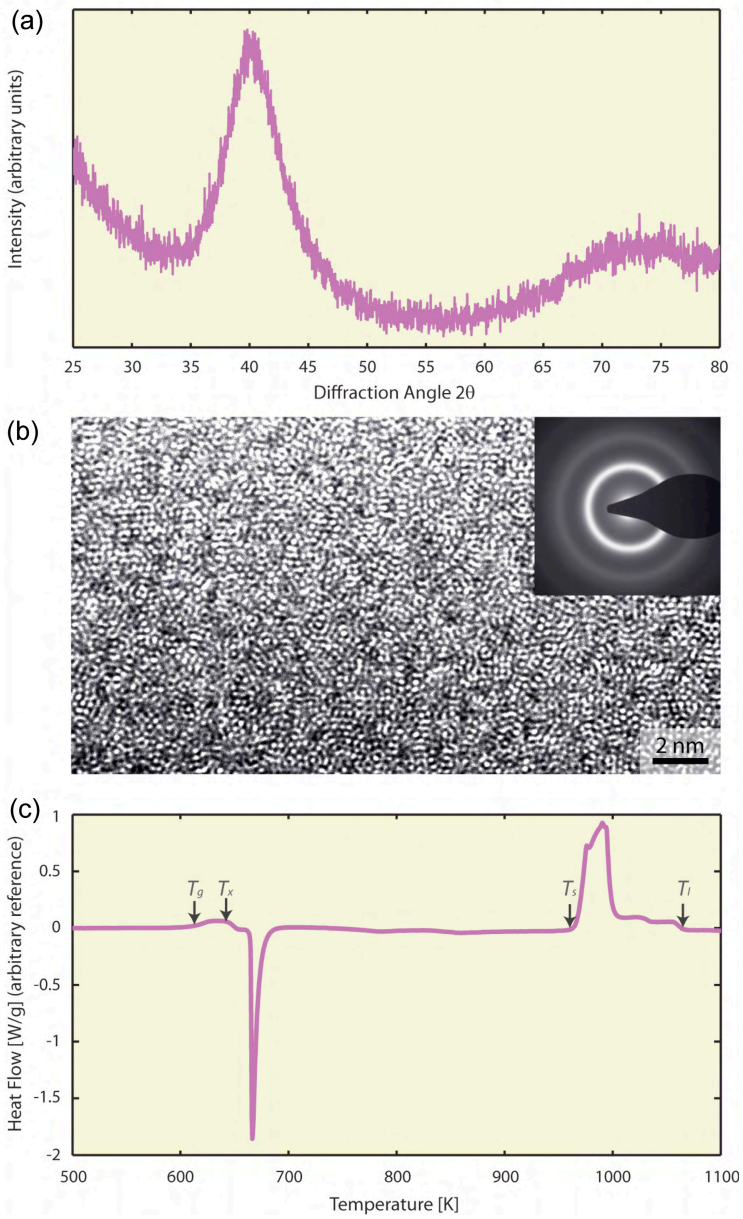

Figure 2.1 Amorphous structure of the $Pd_{79}Ag_{3.5}P_6Si_{9.5}Ge_2$ glass. (a) X-ray diffraction analysis, (b) high-resolution transmission electron microscopy, and (c) differential scanning calorimetry of a bulk $Pd_{79}Ag_{3.5}P_6Si_{9.5}Ge_2$ glassy sample. Arrows in (c) indicate the glass-transition temperature T_g = 613 K, the crystallization temperature T_x = 644 K, the solidus temperature T_s = 967 K, and the liquidus temperature T_l = 1065 K.

UNIAXIAL TENSION TESTING

The amorphous $Pd_{79}Ag_{3.5}P_6Si_{9.5}Ge_2$ tensile-test specimens were produced by water-quenching round tensile-bar-shaped quartz tubes containing the molten alloy. The specimen gauge sections were 1.5 mm in diameter and 20 mm in length. Tests were performed at room temperature with a strain rate of 5×10^{-4} s^{-1} on a screw-driven Instron 5500R testing machine (Instron, Norwood, MA), and strain was recorded using an Epsilon 3448 extensometer. The stress vs. strain loading curve for the bulk glassy sample pulled quasi-statically in uniaxial tension is presented in figure 2.2(a), with corresponding micrographs of the fracture surface in figure 2.2(b). The tensile loading response appears to depart from linear elasticity, and upon yielding, several slip events are evident, see inset in figure 2.2(a). The stress of 1490 MPa marking the first slip event is taken to represent the material plastic yield strength σ_y. Interestingly, a small total plastic strain of ~0.15% was recorded. The corresponding fracture surface figure 2.2(b) is not planar, revealing multiple failure planes (facets), and a large crack offset that did not extend across the gauge section. A ~50 μm wide shear offset is apparent, revealing evidence of extensive "stair like" plastic sliding prior to fracture. These features, which are unusual for tensile failure of a monolithic glass, are consistent with the evidence of limited plasticity recorded in the loading curve. In the absence of a microstructural stabilizing mechanism, however, the attained plasticity cannot properly be termed "ductility"; rather, this extensive multiple plane sliding activity is a demonstration of very high glass toughness.

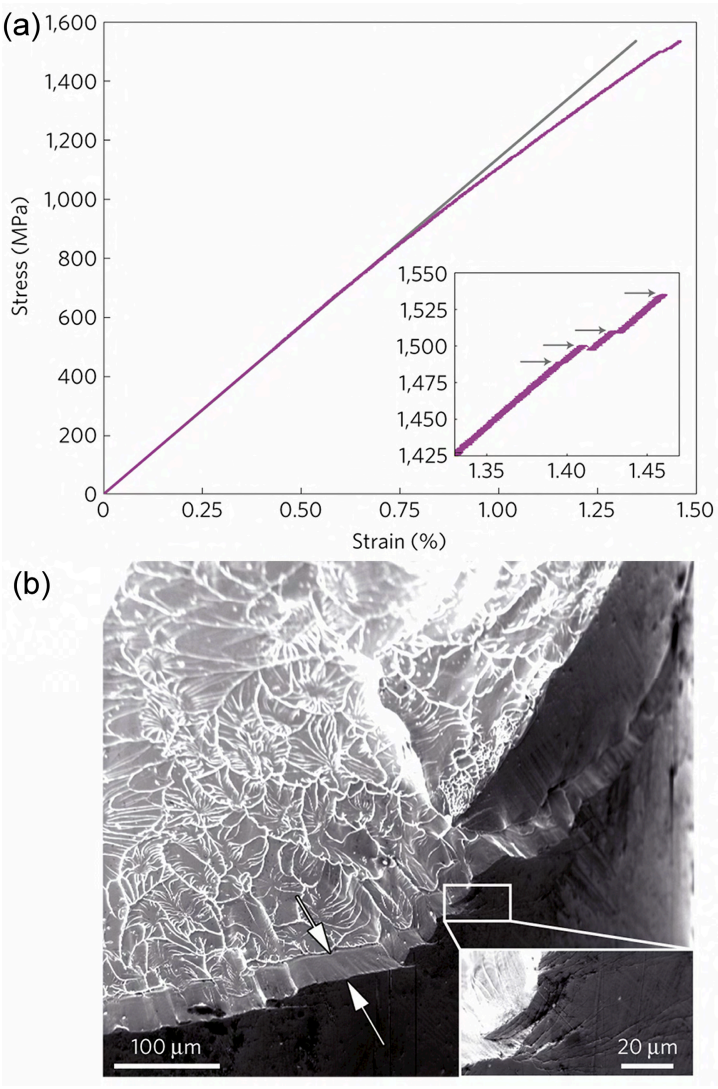

Figure 2.2 Tensile test of the $Pd_{79}Ag_{3.5}P_6Si_{9.5}Ge_2$ glass. (a) Tensile loading curve of a bulk glassy $Pd_{79}Ag_{3.5}P_6Si_{9.5}Ge_2$ specimen. The grey line is a guide for linear elastic response. Inset: Magnified view of the loading curve in the vicinity of yielding. Arrows indicate multiple slip events recorded prior to fracture. (b) Micrograph of the fracture-surface morphology. White arrows designate the shear-sliding offset width. Inset: Magnified view in the vicinity of a shear step revealing dense shear band activity.

FRACTURE TOUGHNESS CHARACTERIZATION

Assessing the fracture toughness of metallic glasses showing extensive plasticity can be extremely challenging, because meeting the fracture-mechanics requirements for linear-elastic *K*–field dominance and the development of plane-strain conditions demands specimen sizes that often exceed the critical thickness for glass formation. For example, measurement of a linear-elastic K_{IC} value of 200 MPa·m$^{1/2}$ requires sample dimensions (in terms of crack size, ligament depth, and thickness; see ASTM Standard E399 [22]) in excess of 45 mm to be considered valid; such dimensions exceed the critical casting thickness of even robust metallic bulk-glass formers. While single-value toughness measurements such as K_{IC} properly define the toughness for crack initiation in brittle materials, they are not always sufficient to characterize the toughness of glassy metals demonstrating extensive plastic yielding, or exhibiting toughening mechanisms that result in significant subcritical crack growth prior to unstable fracture [23]. The nonlinear elastic *J* measurement, which is the appropriate testing method for elastic-plastic materials, has much less restrictive specimen size validity criteria (in terms of crack size, ligament depth, and thickness; see ASTM Standard E1820 [24]) than K_{IC} measurements. A J_C value of 450 kJ/m^2 and yield strength value of 1500 MPa has a thickness and uncracked ligament requirement of 3 mm, but that is still slightly larger than is experimentally convenient. To overcome the large sample size constraints for meeting the small-scale yielding conditions while still properly accounting for the extension of the crack, we here implement a crack-tip opening displacement (CTOD) approach. This method allows us to test even smaller bending bars but still attain valid fracture toughness measurements. Specifically, this is a

nonlinear-elastic fracture mechanics methodology where measurements of CTOD, δ_t, can be related to the *J*-integral by [25]

$$J = d_n \sigma_o \delta_t, \tag{1}$$

where σ_o is defined as the flow stress (the average of the yield and ultimate stresses), and d_n is a constant tabulated from the strain-hardening exponent, *n*, of the material [25]. A finite *n* is essential for the *J*-field to dominate over some finite region. It is well established that metallic glasses strain soften locally on yielding (i.e., within an operating shear band). When metallic glass is subjected to pure tension, the glass typically fails along a single shear band by unconstrained slipping, and no global strain hardening is generally detectable. However, when metallic glass is subjected to a quasi-stable loading geometry such as bending, there is a stress gradient from tension to compression across the sample where generated shear bands can propagate from the tensile surface to the neutral axis, multiply in number, and intersect with each other. The intersection and multiplication of shear bands generally gives rise to compatibility stresses between deformed and undeformed regions, which induces a small global hardening effect that is detectable in the true stress-strain response. For the toughness measurements, this limited degree of strain hardening occurring at the continuum scale is essentially sufficient to ensure "CTOD dominance" at the crack tip.

To determine the hardening exponent *n* of the $Pd_{79}Ag_{3.5}P_6Si_{9.5}Ge_2$ glass in bending, a 2.1 mm by 2.1 mm square bar sample was mechanically ground from a 3 mm diameter rod. The bar was not notched prior to testing. The three-point bending test was performed

on a servo-hydraulic testing machine (MTS, Eden Prairie, MN) at a displacement rate of 10 μm·s^{-1} with a support span of 15 mm. At this sample size and strain rate, we can calculate a n from quantitative stress-strain information that is appropriate and valid for use in our CTOD fracture toughness measurements, thus ensuring that the J-field crack-tip uniqueness is preserved. Post test secondary-electron images of the unnotched bending sample are shown in figure 2.3. A great deal of shear banding can be seen in figure 2.3, both on the compression and tension side of the sample. Shear offsets of up to 200 μm can be seen in figure 2.3(d) (shown by the arrow). A crack propagated from the tension side all the way to the center of the beam, but the sample did not fracture catastrophically even after undergoing 14% bending strain. The bending fixture actually ran out of travel distance and was unable to apply any more strain. The engineering stress vs. strain curve is shown in figure 2.4 and it appears that there is no strain hardening response, only a serration at 11% strain where the crack emerges and propagates to the neutral axis of the beam. However, when inspecting the true stress vs. strain curve also in figure 2.4, it is apparent that there is a slight strain hardening response in the region before the crack emerges. The strain-hardening exponent n was measured by fitting the true stress with the relationship $\sigma_T = C\varepsilon_T^n$, where σ_T is the true stress, ε_T is the true strain, and C is a constant. The glassy $Pd_{79}Ag_{3.5}P_6Si_{9.5}Ge_2$ unnotched bending sample displays a small degree of apparent hardening in bending such that $n \approx 0.13$, ensuring dominance of CTOD at the crack tip and the appropriateness in using equation 1.

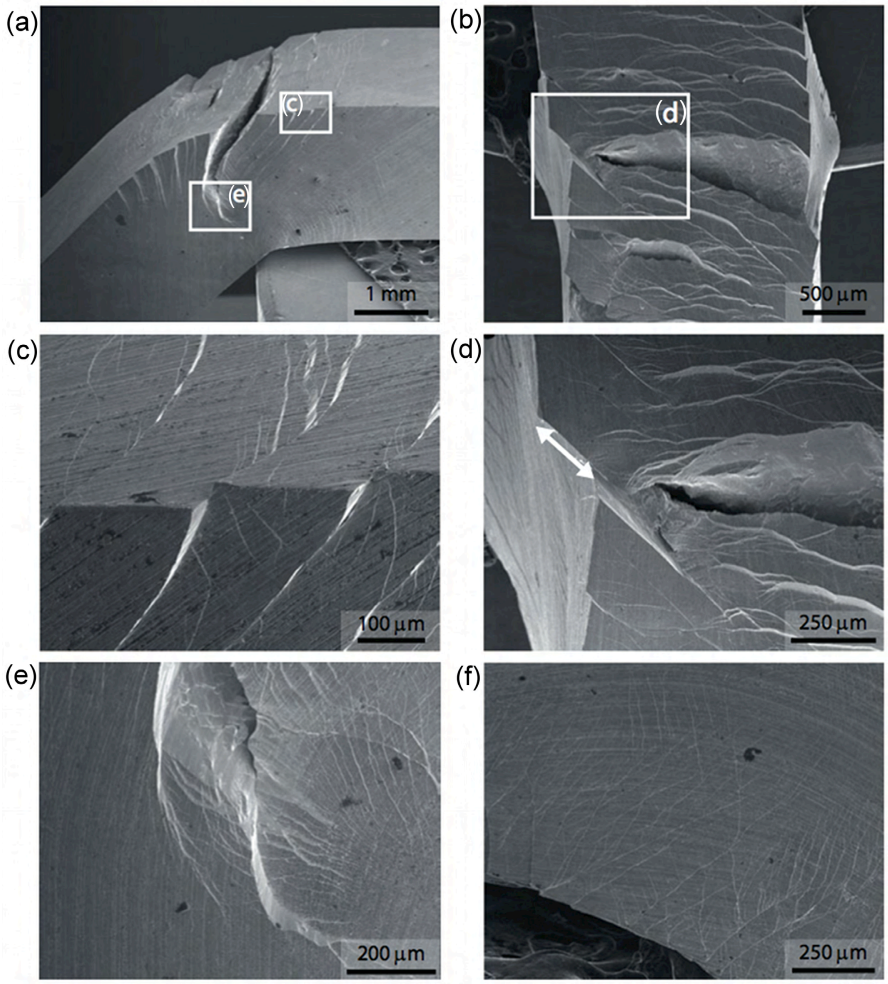

Figure 2.3 Secondary electron micrographs taken after a three-point bending test on an unnotched $Pd_{79}Ag_{3.5}P_6Si_{9.5}Ge_2$ glassy specimen. (a, b) A dense network of shear bands is observed in the tension side of the specimen along with an open crack that propagated in a stable fashion toward the center of the beam. The sample did not fracture catastrophically after undergoing the entire bending strain applicable by the fixture; (c, d) Shear offsets in the tension side are shown, that appear to be as long as 200 µm (see arrow in d). (e) Plastic-flow stabilization at the crack tip promoting stable crack growth, and (f) plastic flow in the compression side.

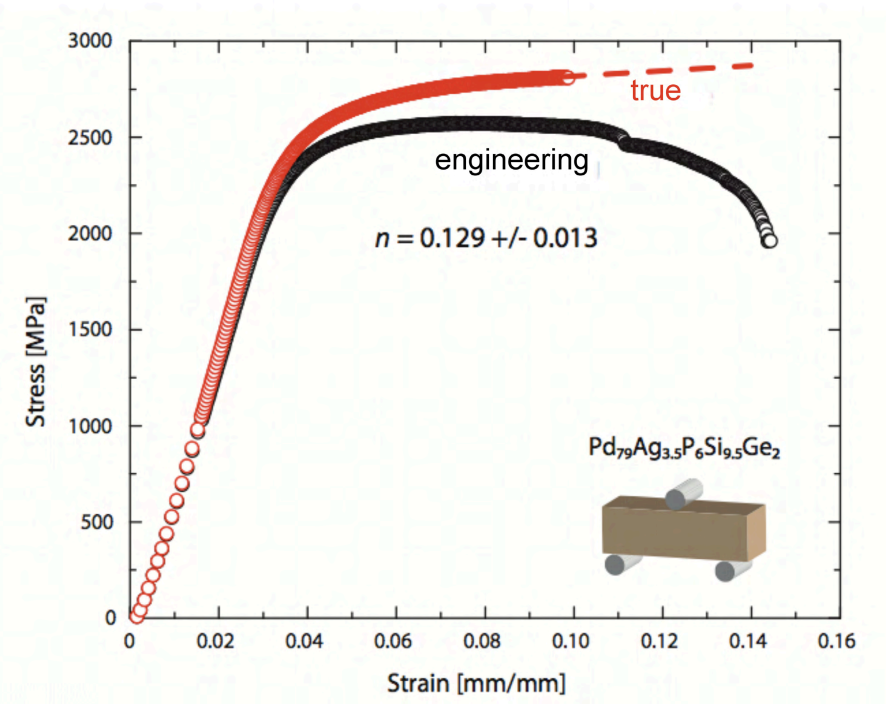

Figure 2.4 Engineering and true stress-strain curve for an unnotched $Pd_{79}Ag_{3.5}P_6Si_{9.5}Ge_2$ glassy specimen tested in a three-point bending configuration. The serration at ~11% strain (engineering curve) marks the development of the crack seen in figure 2.3, and the decreasing loading response following the serration reflects the loss of rigidity due to crack extension. The sample did not fracture catastrophically after undergoing 14% bending strain (see figure 2.3). A slight hardening response is evident in the true stress-strain curve, which can be attributed to multiplication and intersection of shear bands giving rise to local compatibility stresses.

Now that we have determined glassy $Pd_{79}Ag_{3.5}P_6Si_{9.5}Ge_2$ has a finite strain-hardening exponent, we can look at the CTOD testing method in more detail. During a fracture toughness test CTOD δ_t, crack extension Δa, and applied load are measured at regular intervals. The crack-tip opening displacement, δ_t, was measured graphically as the opening distance between the intercept of two 45° lines drawn back from the tip with the deformed profile, shown in figure 2.5, as derived by Shih [25] from the Hutchinson-Rice-Rosengren (HRR) singularity [25-28]. At each interval i, δ_t is defined as:

$$\delta_t = \delta_i - \delta_o, \tag{2}$$

where δ_i is the actual crack-tip opening displacement and δ_o is the initial crack-tip opening displacement before loading. J values were then calculated using Eq. 1 for each crack increment and converted to equivalent K values through the J-K equivalence relationship for nominally mode I fracture in plane stress:

$$K_J = (JE)^{1/2}, \tag{3}$$

with E = 88 GPa the Young's modulus of the $Pd_{79}Ag_{3.5}P_6Si_{9.5}Ge_2$ glass.

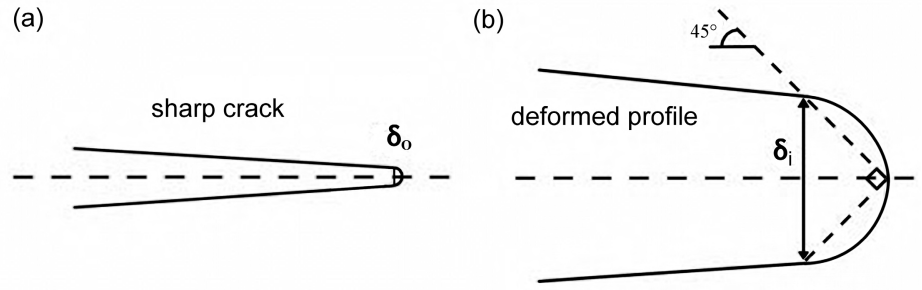

Figure 2.5 Procedure for defining the crack-tip opening displacement. (a) The initially sharp crack and (b) the deformed crack profile illustrating the 45° technique for CTOD.

It is important to note that equation (1) is valid for both plane strain and plane stress conditions, and as long as the HRR fields dominate. In the large-scale yielding regime (as in the present case), the size of the region dominated by the singularity fields is dependent on specimen geometry [26]; in this regime, Shih [25] shows that the relationship between J and δ_t, as expressed in equation (1), holds under large-scale plasticity for a hardening material when the uncracked ligament is subjected primarily to bending.

To verify that this CTOD approach is suitable for metallic glasses that undergo extensive plastic yielding, we compared the CTOD estimated K_J value against the K_J value obtained using direct J-integral measurements. It is necessary to do this comparison on a glassy material with a well-known toughness that has extensive plastic yielding in the large-scale yielding regime. Since most monolithic bulk metallic glasses fail catastrophically soon after yielding by unstable crack extension (other than the Pd-based glass of this paper), they do not exhibit rising R-curves (fracture toughness *vs.* crack extension). As an alternative, we use the well-documented R-curve [23] of the ductile-phase-reinforced metallic glass ($Zr_{39.6}Ti_{33.9}Nb_{7.6}Cu_{6.4}Be_{12.5}$) [3]. The comparison between the two methods on $Zr_{39.6}Ti_{33.9}Nb_{7.6}Cu_{6.4}Be_{12.5}$ is shown in figure 2.6. Good agreement was obtained between the two measurement techniques. More importantly, the CTOD method is shown to provide a *conservative* estimate of the toughness (i.e., it slightly underestimates the toughness).

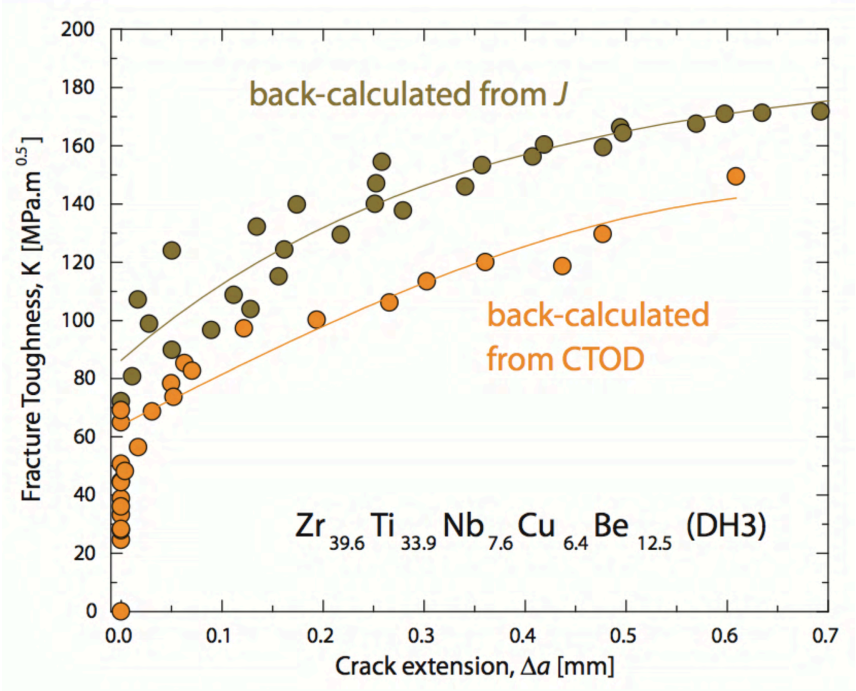

Figure 2.6 Comparison of R-curves derived using direct *J*-integral and CTOD methods for ductile-phase-reinforced metallic glass $Zr_{39.3}Ti_{33.9}Nb_{7.6}Cu_{6.4}Be_{12.5}$. Good agreement between the two measurements techniques is shown. The CTOD approach utilized in the present work can be seen to provide a conservative estimate of the fracture toughness.

Having established the appropriateness and validity of the CTOD testing method for small bending specimens of bulk metallic glass that undergo extensive plastic yielding, we will describe the CTOD testing results for the $Pd_{79}Ag_{3.5}P_6Si_{9.5}Ge_2$ glass. Single-edge notched beam SE(B) rectangular beam specimens were prepared by mechanically grinding 3 mm diameter rods of glass to square beam specimens with a cross section of 2.1 mm by 2.1 mm, and length of 20 mm. Fatigue precracking was rendered impractical here due to the small size of the samples. Instead, a razor-micronotching technique was employed to generate a sharp crack within an acceptable range [29]. The notches were first introduced

using a low-speed diamond saw, and then sharpened using a razor-micronotching technique. Micro-notches with a root radius of ~5 to 10 μm were obtained by repeatedly sliding a razor blade over the saw-cut notch using a custom-made rig, while continually irrigating with a 1 μm diamond slurry. Sharp cracks with an initial crack length a of ~1.0 mm were generated in general accordance with ASTM standard E1820 [24]. Prior to testing, both specimen faces were polished to a 1 μm surface finish with a diamond suspension. In the fracture toughness tests, δ_t vs. Δa fracture toughness resistance curves (R-curves) were measured on three micronotched specimens *in situ* in a Hitachi S-4300SE/N environmental scanning electron microscope (Hitachi America, Pleasanton, CA) using a Gatan Microtest three-point bending stage (Gatan, Abington, UK) with a support span of 15 mm. The crosshead displacement was measured with a linear variable displacement transducer, while the load was recorded using a 2000 N load cell. The CTOD and crack extension were monitored at regular intervals in secondary electron mode *in vacuo* (10^{-4} Pa) at a 20 kV excitation voltage.

Using the CTOD method and experimental setup described above, we have used the CTOD approach to determine the fracture toughness of a metallic glass with critical casting thickness below the width required for direct J-integral toughness measurements. The mode I (tensile opening) fracture toughness R-curve of glassy $Pd_{79}Ag_{3.5}P_6Si_{9.5}Ge_2$ is shown in figure 2.7(a). Results for the stress intensity K_J back-calculated from the J measurements are shown in figure 2.7(b). The glass demonstrates extensive rising R-curve behavior indicative of stable crack growth over hundreds of micrometers. A near steady state K_{Jc} of ~200 MPa·m$^{1/2}$ (J_C ~460 kJ/m^2) is attained. This is an exceptionally high value

for any material, but especially for an inherently non-ductile solid with an entirely amorphous structure. More interestingly, the rising R-curve in figure 2.7(b) indicates that the glass toughens as a crack extends; an attribute of ductile crystalline metals not previously thought possible for an amorphous material.

Mechanistically, we identified the salient sources of toughening in the glass by performing the fracture toughness tests *in situ* in the scanning electron microscope. This technique allows the quantitative measurement of the R-curve while simultaneously monitoring the evolution of damage ahead of the crack tip and the toughening mechanisms in the crack wake. The high toughness value is achieved by stabilizing the plastic flow processes at the opening crack tip to form a distributed damage zone accompanied by significant plastic shielding, see figure 2.7(c–k). The specific mechanisms contributing to the toughness of the $Pd_{79}Ag_{3.5}P_6Si_{9.5}Ge_2$ glass can be described in terms of a three-step process. First, shear bands form along the fan-shaped (Prandtl field) slip lines [30,31] that bend back toward the crack plane, figure 2.7(d–f). Accompanying the development of the Prandtl field, extensive localized shear sliding occurs along the evolved slip planes leading to very large shear offsets shown in figure 2.7(f). When a critical sliding strain is reached with increasing load, the extended shear bands open at the crack tip and then evolve as cracks like in figure 2.7(g). As the slip bands bend back to the crack plane enabling substantial shear sliding, the crack remains stable on its plane such that stable crack extension is attained during fracture, figure 2.7(g–k). It should be noted that outright catastrophic fracture did not occur in any of the specimens under the geometry and conditions considered here.

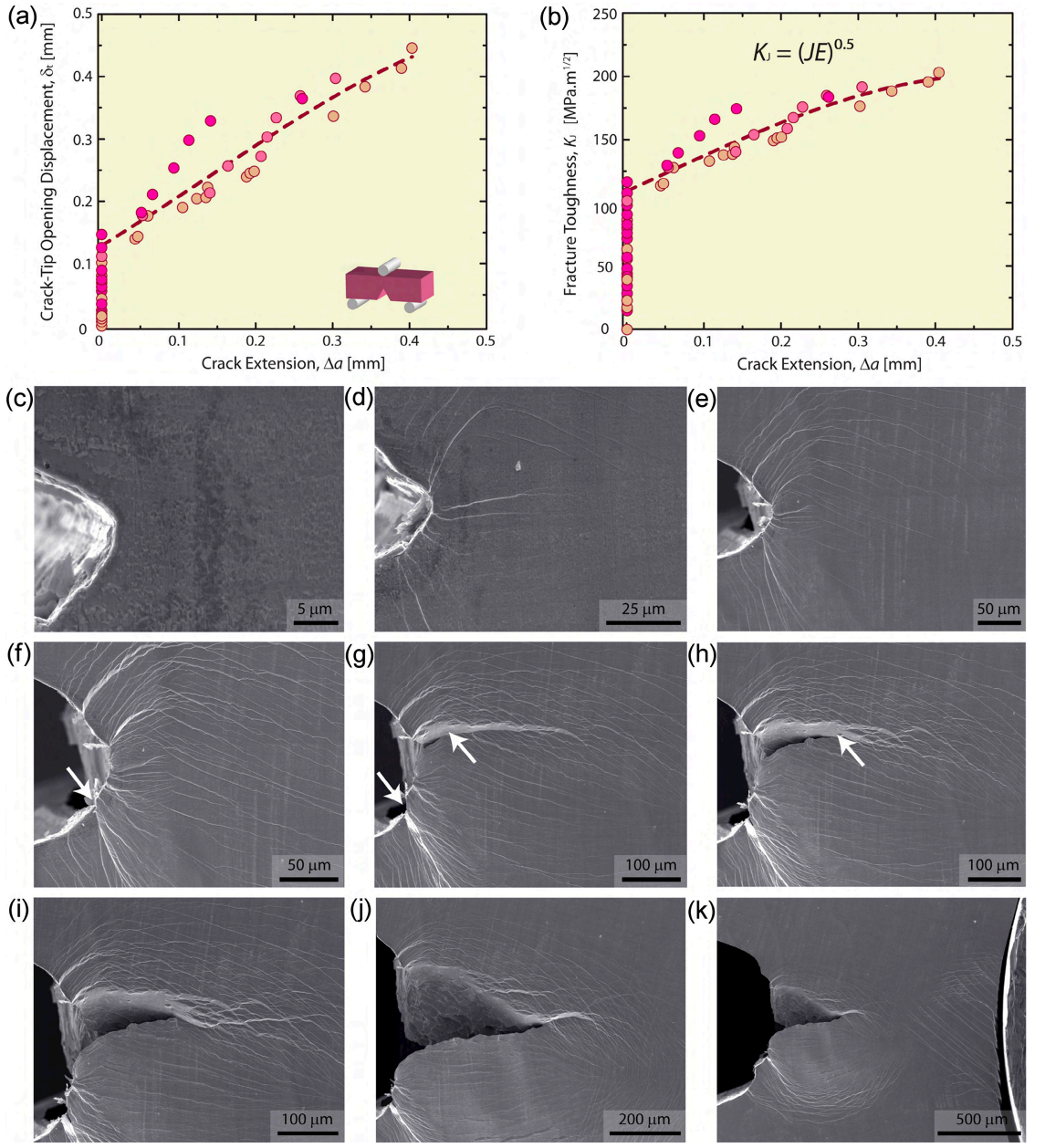

Figure 2.7 Fracture toughness measurements of the $Pd_{79}Ag_{3.5}P_6Si_{9.5}Ge_2$ glass. (a) The crack-tip opening displacement, δ_t, determined graphically, is plotted against the crack extension, Δa. (b) Fracture toughness, K_{Jc}, back-calculated from the *J*–integral, plotted against the crack extension, Δa. The red and orange dots in (a) and (b) represent two different fracture toughness measurements. (c-k) Scanning electron micrographs taken

during an *in situ* R-curve measurement of a SE(B) specimen. The specimen initially contained a sharp notch with a root radius of ~5 μm [25]. The crack-tip opening displacement was measured graphically at regular intervals. The corresponding fracture toughness K values are (c) 0 MPa·m$^{1/2}$ (d) 25 MPa·m$^{1/2}$, (e) 44 MPa·m$^{1/2}$, (f) 63 MPa·m$^{1/2}$, (g) 115 MPa·m$^{1/2}$, (h) 133 MPa·m$^{1/2}$, (i) 144 MPa·m$^{1/2}$, (j) 196 MPa·m$^{1/2}$, (k) 203MPa·m$^{1/2}$. (d,e) Shear bands initiate at relatively low stress intensity values along the Prandtl slip lines. (f,g) An increase in K_J is recorded associated with extensive shear sliding (indicated by arrows) that generates significant crack tip blunting. (h–k) At high stress, a crack initiates by opening of a shear band and subsequently extends at stable rate. Image (k) depicts the state of the specimen at the end of the test, showing that the sample did not fracture catastrophically after undergoing the entire strain applicable by the fixture.

Even though the mechanisms controlling the plastic zone development in the present glass are not fundamentally different than in other metallic glasses, the characteristic length scales associated with such development are considerably larger. The shear sliding process under an opening stress, which constitutes the key mechanism of plastic zone development, is illustrated schematically in figure 2.8(a). Although all metallic glasses are generally capable of undergoing limited shear band sliding in the presence of a flaw, the extent of shear sliding and observed shear offsets seen in the present glass are unprecedented. As shown in figure 2.8(b), shear offsets as large as 50 μm are attained prior to crack opening. These extended offsets enable the buildup of a very large plastic zone prior to cavitation and crack extension. The homogeneous plane-stress plastic

zone radius of the $Pd_{79}Ag_{3.5}P_6Si_{9.5}Ge_2$ glass can be estimated to be as large as $r_p = K_c^2/\pi\sigma_y^2$ ≈ 6 mm. This value is the largest measured in monolithic metallic glass and rivals that of the ductile-phase-reinforced metallic glasses [3]. It also compares well with plastic zone sizes of common crystalline engineering metals.

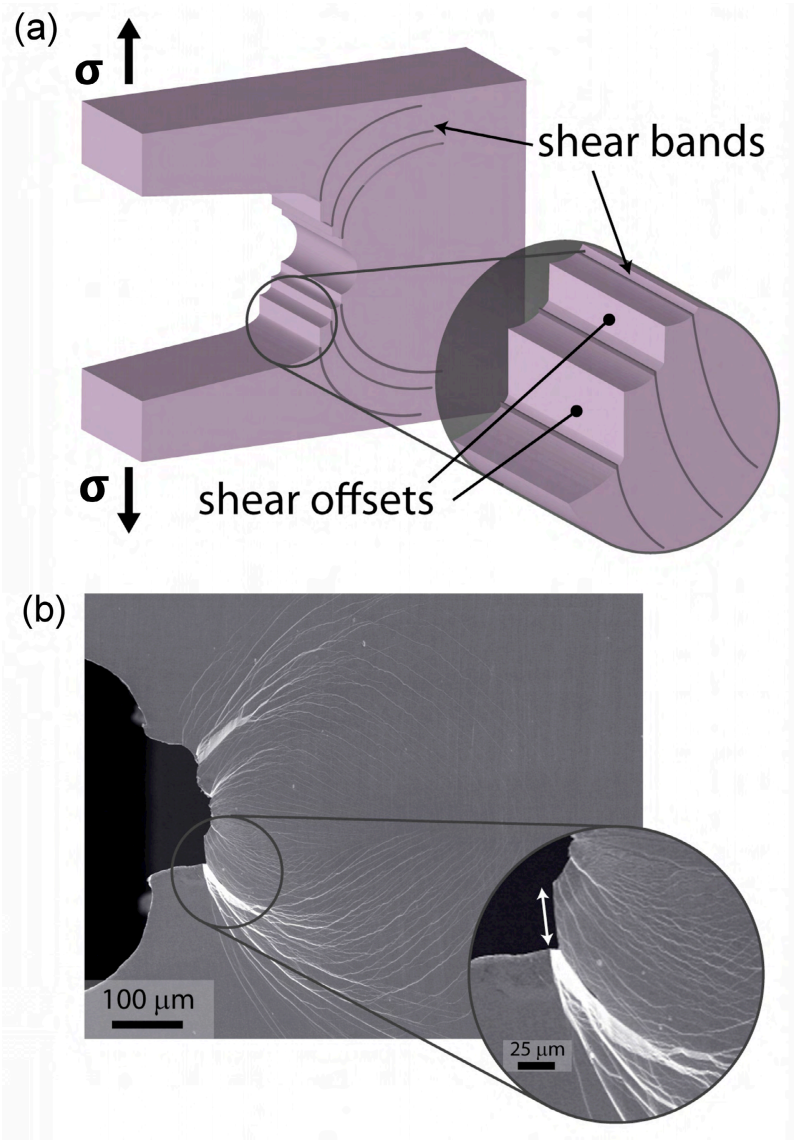

Figure 2.8 Shear-sliding mechanism governing metallic glass toughness. (a) Schematic illustrating the process of crack blunting through shear sliding in the vicinity of a flaw

under opening stress. (b) Micrograph of a deformed notch in a glassy $Pd_{79}Ag_{3.5}P_6Si_{9.5}Ge_2$ specimen showing extensive plastic shielding of an initially sharp crack. Inset: Magnified view revealing a 50 μm shear offset (arrow) developed during plastic sliding prior to the onset of crack opening

TOUGHNESS CORRELATION

To investigate the self-similarity in plastic zone development extending over several orders of magnitude in size for the various metallic glass systems, a scaling law is introduced. The number of net activated shear transformation events prior to a cavitation event in the core of an operating shear band is described here by a dimensionless parameter f, defined as $f = \exp[-(W_s - W_c)/k_BT]$, where W_s and W_c are the activation energy barriers for shear flow and cavitation respectively, and T is a reference temperature. The glass-transition temperature of the amorphous material is recognized to be a good measure of the shear flow barrier; specifically, $W_s \approx 37k_BT_g$ [14,32,33]. By further assuming that the ratio of the barrier heights W_c/W_s is dominated by the ratio of the respective elastic curvatures B/G, where B and G are the bulk and shear modulus respectively, one can arrive at the following relation for f:

$$\log\left(\frac{K_C^2}{\pi\sigma_y^2}\right) \sim \log(f) \sim \frac{W_S}{k_BT}\left(\frac{W_C}{W_S} - 1\right) \approx \frac{T_g}{T}\left(\frac{B}{G} - 1\right). \qquad (4)$$

In the above expression, T_g is the glass transition temperature, T is a reference temperature (here taken to be the test temperature, i.e., T = 300 K), G the shear modulus, B the bulk modulus, and $K_c^2/\pi\sigma_y^2$ is the plastic zone radius r_p. Interestingly, the ratio of bulk to shear modulus B/G (or equivalently, the Poisson's ratio) has been previously identified to be a key parameter associated with the toughness of a metallic glass [5,9]. This ratio alone, however, is not adequate to describe the number of net activated shear events, as it does not take into account the absolute magnitude of the activation barriers (here approximated as $\sim k_B T_g$). Using equation (1), f is estimated for a set of ten metallic glass alloys (including the present one) with toughness values that vary over two orders of magnitude, see Table 1 for the complete set of data [7,9,14,34-44]. The estimated f for the present glass is found to be higher than the other glasses, consistent with its larger plastic zone and higher toughness. In fact f, which is formulated to describe the capacity for shear flow prior to cavitation, is found to display a one-to-one correspondence with r_p. As shown in figure 2.9, parameter f correlates with r_p reasonably well, thereby describing the plastic zone development of plastically yielding glasses over four orders of magnitude in size. Based on the correlation in figure 2.9, one may conclude that the very high fracture resistance demonstrated by the present glass is attributed to a large absolute difference between W_s and W_c, as quantified by the high B/G and T_g values for this glass used equation (4). Correspondingly, we believe that this scaling law with B, G, and T_g as design variables (all of which are experimentally accessible) can serve as a viable guide for the development of a new generation of highly fracture-resistant structural glasses.

Glass-Forming Alloy	G [GPa]	B [GPa]	T_g [K]	s_y [MPa]	K_c [MPa.m$^{1/2}$]	References
$Mg_{65}Cu_{25}Tb_{10}$	19.6	44.71	415	660	2	*7,34*
$La_{55}Al_{25}Ni_5Cu_{10}Co_5$	15.6	44.2	430	700	5	*7,14,35*
$Fe_{58}Co_{6.5}Mo_{14}C_{15}B_6Er_{0.5}$	74.0	177.0	790	3700	26.5	*36,37*
$Fe_{66}Cr_3Mo_{10}C_{10}B_3P_8$	66.5	172.0	721	3100	39.3	*36,38*
$Fe_{70}Ni_5Mo_5C_5B_{2.5}P_{12.5}$	57.3	150.1	696	2670	49.8	*39*
$Zr_{55}Cu_{30}Ni_5Al_{10}$	34.7	117.9	684	1650	43.3	*40-42*
$Zr_{41.2}Ti_{13.8}Cu_{12.5}Ni_{10}Be_{22.5}$	34.1	114.1	618	1850	55	*7,43*
$Cu_{60}Zr_{20}Hf_{10}Ti_{10}$	36.9	128.2	754	1950	67.6	*44*
$Pt_{57.5}Cu_{14.7}Ni_{5.3}P_{22.5}$	33.3	198.7	508	1400	81.5	*9*
$Pd_{79}Ag_{3.5}P_6Si_{9.5}Ge_2$	31.1	171.6	613	1490	203	Present

Table 1: Data for ten metallic glass systems used in the correlation given by equation (4).

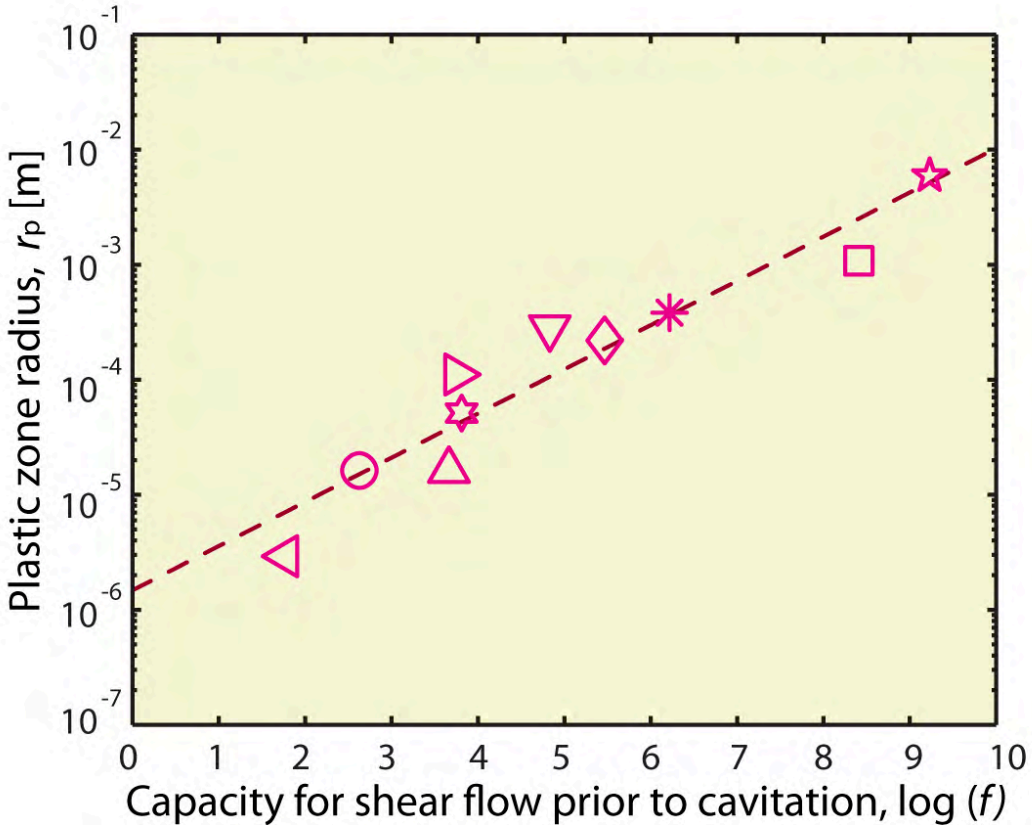

Figure 2.9 Logarithm of the plastic zone radius, defined as $K_c^2/\pi\sigma_y^2$, plotted against the estimated capacity for shear flow prior to cavitation, approximated by $-(W_s - W_c)/K_BT$ from

equation (4). Data for ten metallic glass alloys listed in Table 1 are plotted. Symbols designate the following alloys: (◁) $Mg_{65}Cu_{25}Tb_{10}$; (○) $La_{55}Al_{25}Ni_5Cu_{10}Co_5$; (△) $Fe_{58}Co_{6.5}Mo_{14}C_{15}B_6Er_{0.5}$; (✡) $Fe_{66}Cr_3Mo_{10}C_{10}B_3P_8$; (▷) $Fe_{70}Ni_5Mo_5C_5B_{2.5}P_{12.5}$; (◇) $Zr_{55}Cu_{30}Ni_5Al_{10}$; (▽) $Zr_{41.2}Ti_{13.8}Cu_{12.5}Ni_{10}Be_{22.5}$; (✸) $Cu_{60}Zr_{20}Hf_{10}Ti_{10}$; (□) $Pt_{57.5}Cu_{14.7}Ni_{5.3}P_{22.5}$; (☆) $Pd_{79}Ag_{3.5}P_6Si_{9.5}Ge_2$. Line is a regression to the data.

ASHBY DAMAGE TOLERANCE MAP

The values of fracture energy and toughness presented here for glassy $Pd_{79}Ag_{3.5}P_6Si_{9.5}Ge_2$ are comparable to values for the toughest engineering metals known (e.g., low-carbon steels). Considering that a glass lacks microstructural defects like dislocations, which rearrange to shield stress and suppress crack opening, achieving such high fracture resistance is quite remarkable. Moreover, in sharp contrast to tough crystalline metals, the absence of defects enables the very high strength associated with the amorphous structure. Thus, an unusual combination of very high strength and toughness (i.e., very high damage tolerance) is possible, a feature perhaps unparalleled by any known monolithic material. In figure 2.10 we present an Ashby map [45] showing toughness vs. strength ranges for oxide glasses, engineering ceramics, engineering polymers, and engineering metals, along with data for monolithic metallic glasses (including the present glass) and ductile-phase reinforced metallic glasses. As shown in the map, the toughness vs. strength data for the present glass lies outside the benchmarks established by the strongest and toughest steels. In summary, the present results demonstrate that the

combination of toughness and strength (i.e., the level of damage tolerance) potentially accessible to amorphous materials extends beyond the traditional limiting ranges toward levels previously inaccessible to any material.

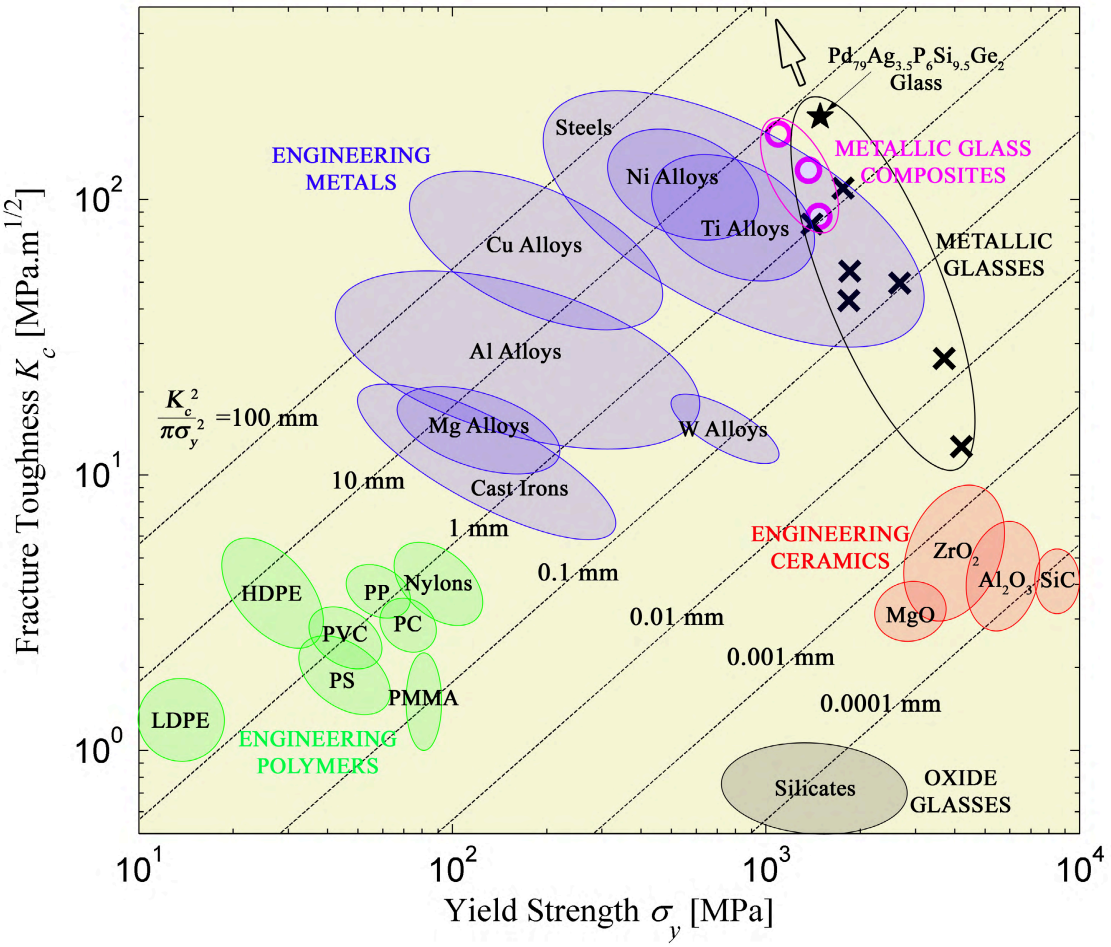

Figure 2.10 Ashby map of the damage-tolerance (toughness vs. strength) of materials. Ranges of fracture toughness vs. yield strength are shown for oxide glasses [45], engineering ceramics [45], engineering polymers [45], and engineering metals [45], along with data for the $Pd_{79}Ag_{3.5}P_6Si_{9.5}Ge_2$ glass designated by symbol (★), data for other metallic glasses: three Fe-based glasses [36,39], two Zr-based glasses [40,43], a Ti-based glass [11], and a Pt-based glass [9] all designated by symbol (×). Data for ductile-phase-

reinforced metallic glasses [3] is designated by symbol (○). Yield strength data shown for oxide glasses and ceramics represent ideal limits. Contours correspond to values for the plastic zone radius, $K_c^2/\pi\sigma_y^2$, in mm. As indicated by the arrow, the combination of toughness and strength (i.e., damage tolerance) potentially accessible to metallic glasses extends beyond the traditional limiting ranges toward levels previously inaccessible to any material.

BIBLIOGRAPHY

[1] M. E. Launey and R. O. Ritchie, Adv Mater **21**, 2103 (2009).

[2] R. O. Ritchie, Science **320**, 448 (2008).

[3] D. C. Hofmann, J.-Y. Suh, A. Wiest, G. Duan, M. L. Lind, M. D. Demetriou, and W. L. Johnson, Nature **451**, 1085 (2008).

[4] M. F. Ashby and A. L. Greer, Scripta Materialia **54**, 321 (2006).

[5] J. J. Lewandowski, W. H. Wang, and A. L. Greer, Philosophical Magazine Letters **85**, 77 (2005).

[6] J. Xu, U. Ramamurty, and E. Ma, Jom-Us **62**, 10 (2010).

[7] X. K. Xi, D. Q. Zhao, M. X. Pan, W. H. Wang, Y. Wu, and J. J. Lewandowski, Phys Rev Lett **94**, 125510 EP (2005).

[8] P. A. Hess, S. J. Poon, G. J. Shiflet, and R. H. Dauskardt, Journal of Materials Research **20**, 783 (2005).

[9] J. Schroers and W. Johnson, Phys Rev Lett **93**, (2004).

[10] J.-Y. Suh, R. D. Conner, C. P. Kim, M. D. Demetriou, and W. L. Johnson, Journal of Materials Research **25**, 982 (2010).

[11] X. J. Gu, S. J. Poon, G. J. Shiflet, and J. J. Lewandowski, Acta Mater **58**, 1708 (2010).

[12] A. Inoue, B. Shen, H. Koshiba, H. Kato, and A. R. Yavari, Nat Mater **2**, 661 (2003).

[13] R. Conner, W. Johnson, N. Paton, and W. Nix, J Appl Phys **94**, 904 (2003).

[14] W. Johnson and K. Samwer, Phys Rev Lett **95**, 195501 (2005).

[15] E. Bouchaud, D. Boivin, J. L. Pouchou, D. Bonamy, B. Poon, and G. Ravichandran, Epl-Europhys Lett **83**, (2008).

[16] P. Duwez, R. H. Willens, and R. C. Crewdson, J Appl Phys **36**, 2267 (1965).

[17] H. S. Chen, J. T. Krause, and E. Coleman, J Non-Cryst Solids **18**, 157 (1975).

[18] H. S. Chen and D. Turnbull, Acta Metallurgica **17**, 1021 (1969).

[19] H. Kimura and T. Masumoto, Acta Metallurgica **28**, 1663 (1980).

[20] H. Kimura and T. Masumoto, Acta Metallurgica **28**, 1677 (1980).

[21] H. W. Kui, A. L. Greer, and D. Turnbull, Appl Phys Lett **45**, 615 (1984).

[22] *ASTM Standard E399* (ASTM International, West Conshohocken, PA, 2012).

[23] M. E. Launey, D. C. Hofmann, J. Y. Suh, H. Kozachkov, W. L. Johnson, and R. O. Ritchie, Appl Phys Lett **94**, 241910 (2009).

[24] *ASTM Standard E1820* (ASTM International, West Conshohocken, PA, 2011).

[25] C. F. Shih, J Mech Phys Solids **29**, 305 (1981).

[26] C. F. Shih and M. D. German, International Journal of Fracture **17**, 27 (1981).

[27] J. W. Hutchinson, Acta Mater **16**, 337 (1968).

[28] J. R. Rice and G. F. Rosengren, Acta Mater **16**, 1 (1968).

[29] P. Lowhaphandu and J. J. Lewandowski, Scripta Materialia **38**, 1811 (1998).

[30] A. Alpas, L. Edwards, and C. Reid, Metall and Mat Trans A **20**, 1395 (1989).

[31] K. M. Flores and R. H. Dauskardt, Scripta Materialia **41**, 937 (1999).

[32] M. D. Demetriou, J. S. Harmon, M. Tao, G. Duan, K. Samwer, and W. L. Johnson, Phys Rev Lett **97**, (2006).

[33] W. L. Johnson, M. D. Demetriou, J. S. Harmon, M. L. Lind, and K. Samwer, Mrs Bull **32**, 644 (2007).

[34] X. Xi, D. Zhao, M. Pan, and W. Wang, J Non-Cryst Solids **344**, 189 (2004).

[35] N. Nagendra, U. Ramamurty, T. T. Goh, and Y. Li, Acta Mater **48**, 2603 (2000).

[36] A. Shamimi Nouri, X. J. Gu, S. J. Poon, G. J. Shiflet, and J. J. Lewandowski, Philosophical Magazine Letters **88**, 853 (2008).

[37] X. J. Gu, S. J. Poon, and G. J. Shiflet, Journal of Materials Research **22**, 344

(2007).

[38] X. J. Gu, S. J. Poon, G. J. Shiflet, and M. Widom, Appl Phys Lett **92**, 161910 (2008).

[39] M. D. Demetriou, G. Kaltenboeck, J.-Y. Suh, G. Garrett, M. Floyd, C. Crewdson, D. C. Hofmann, H. Kozachkov, A. Wiest, J. P. Schramm, and W. L. Johnson, Appl Phys Lett **95**, 041907 (2009).

[40] A. Kawashima, H. Kurishita, H. Kimura, and T. Zhang, Materials Transactions **46**, 1725 (2005).

[41] J. Luo, H. Duan, C. Ma, S. Pang, and T. Zhang, Materials Transactions **47**, 450 (2006).

[42] M. L. Vaillant, V. Keryvin, T. Rouxel, and Y. Kawamura, Scripta Materialia **47**, 19 (2002).

[43] C. J. Gilbert, R. O. Ritchie, and W. L. Johnson, Appl Phys Lett **71**, 476 (1997).

[44] P. Wesseling, T. G. Nieh, W. H. Wang, and J. J. Lewandowski, Scripta Materialia **51**, 151 (2004).

[45] M. F. Ashby, *Materials Selection in Mechanical Design* (Pergamon Press, Oxford; New York, 1992).